Available online at www.sciencedirect.com
ScienceDirect
Ceramics International 37 (2011) 2127–2134
CERAMICS INTERNATIONAL
www.elsevier.com/locate/ceramint

Electrical conduction behaviors of isovalent and acceptor dopants on B site of $(La_{0.8}Ca_{0.2})CrO_{3-\delta}$ perovskites

Yen-Pei Fu [a,*], Hsin-Chao Wang [a], Shao-Hua Hu [b], Kok-Wan Tay [c]

[a] Department of Materials Science and Engineering, National Dong-Hwa University, Shou-Feng, Hualien 974, Taiwan
[b] Department of Environmental Resources Management, Dahan Institute of Technology, Sincheng, Hualien 971, Taiwan
[c] Department of Electronic Engineering, Wu-Feng University, Minhsiung, Chiayi 621, Taiwan

Received 14 September 2010; received in revised form 27 January 2011; accepted 28 February 2011
Available online 8 April 2011

Abstract

The electrical conduction behaviors of isovalent and acceptor dopants on B site of $(La_{0.8}Ca_{0.2})CrO_{3-\delta}$ perovskites at high and low oxygen activities were investigated systematically. In this study, the concept of defect chemistry is used to explain the relationship between the concentration of electron hole with the electrical conductivity. The information of charge compensation mechanisms and defect formation may be valuable for a better understanding of the interconnect of $(La_{0.8}Ca_{0.2})CrO_{3-\delta}$-based ceramics used for solid oxide fuel cells (SOFCs). Since $(La_{0.8}Ca_{0.2})CrO_{3-\delta}$-based specimens belong to p-type conductors, their conductivities are proportional to the concentration of electron hole. In reducing atmosphere, the oxygen may be lost and ionic compensation may be take place through the formation of oxygen vacancies and the electrical compensation may arise by changing the valence of Cr from tri-valence to tetra-valence in reducing atmosphere. However the formation of oxygen vacancies has no contribution to electrical conductivity, the compensation mechanism is dominated by the electrical compensation, *i.e.* the take place a transition of $Cr^{3+} \rightarrow Cr^{4+}$ rather than that of ionic compensation, *i.e.* the formation of oxygen vacancies. Based on the defect chemical reactions and the results of electrical conductivity, the concentration of electron hole at high oxygen activity is larger than that at low oxygen activity. Therefore the electrical conductivity of $(La_{0.8}Ca_{0.2})CrO_{3-\delta}$-based ceramics at air is larger than that at 5% H_2–95% Ar forming gas. The compensation mechanisms contain ionic and electrical compensation and the ratios of electrical to ionic compensation varied with the kind of dopant which significantly effects the electrical conductivity. The results suggest that the $(La_{0.8}Ca_{0.2})Cr_{0.9}Co_{0.1}O_{3-\delta}$ specimen shows high electrical conductivity in air ($\sigma_{850\ ^\circ C}$ = 59.59 S/cm) and 5% H_2–95% Ar forming gas ($\sigma_{850\ ^\circ C}$ = 47.98 S/cm) leading it a promising candidate as an interconnect material for SOFCs applications.

Keywords: A. Powder: solid state reaction; C. Electrical conductivity; D. Perovskites; E. Fuel cells

1. Introduction

Solid oxide fuel cells (SOFCs) are one of the most realistic candidates for a new generation power system due to its high energy conversion efficiency, environmental compatibility and ability to use hydrocarbon fuels directly without external reforming [1,2]. Many of the challenges in the development of SOFCs can be met with improved materials. The interconnect materials, which provide the conductive path for electrical current to pass between the electrodes and to the external circuit, are critical materials in SOFCs. Regardless of planar or tubular cell configuration, the role of an interconnect material is actually twofold: it provides an electrical connection between the anode of one individual cell to the cathode of the adjoining one and it acts as a physical barrier to protect the air electrode material from the reducing environment of the fuel on the fuel electrode side, and to prevent the fuel electrode material from being in contact with the oxidizing atmosphere of the air electrode side [3–5]. Depending on the operating temperature either a ceramic or a metallic interconnect is used. Ceramics interconnects are used when the operating temperature is above 900 °C, while the metallic interconnects are used when the operating temperature is below 800 °C [6]. Each type of interconnect has its own merits and demerits. Although metallic interconnects have high electrical conductivity, they have a tendency toward oxidation under oxidizing conditions at the

* Corresponding author. Tel.: +886 3 863 4209; fax: +886 3 863 4200.
E-mail address: d887503@alumni.nthu.edu.tw (Y.-P. Fu).

0272-8842/$36.00
doi:10.1016/j.ceramint.2011.02.028

cathode site and require protective coating to avoid oxidation [7]. Ceramic interconnects have lower electrical conductivity than that of metallic interconnects, but their electrical conductivity is reasonably good under an oxidizing as well as reducing environment due to their thermal and chemical stability.

Lanthanum chromite substituted with alkaline metals (Ca or Sr) has been widely used for interconnection materials in the present generation of SOFCs [8,9]. However, there are several problems associated with these perovskite materials: (i) poor sinterability in air due to the volatilization of Cr, (ii) insufficiently high electrical conductivity, and (iii) mismatching of the thermal expansion coefficients (TECs) with other SOFC components. To reduce the previously mentioned disadvantages, some researchers have studied this material by substituting alkaline earth metal ions or transition metal ions at the La and Cr sites, respectively [10–14]. In previous works, there have been many investigations on the effects of crystal structure, microstructure, and electrical conductivity behaviors for ionic substitutions for the A sites and B sites behavior. Oishi et al. [15,16] have examined the oxygen nonstoichiometry of B-site doped $LaCrO_3$ as a function of oxygen partial pressure at 700–1100 °C and reported the related information as follows: (1) 10 mol% of dopant in B-site drastically affects the redox property of $LaCrO_3$; (2) Oxygen vacancy formation in $(La_{0.7}Sr_{0.3})(Cr_{1-y}Ti_y)O_{3-\delta}$ ($y = 0.1$ and 0.2) and $(La_{0.7}Sr_{0.3})(Cr_{0.7}Ti_{0.3})O_{3-\delta}$ was explained by redox reaction of Cr and Ti ions, respectively. Hilpert et al. [17] have examined the characteristic properties of A-site and B-site doped $LaCrO_3$ as a function of oxygen partial pressure at 900–1100 °C and reported the effect of the macroscopic mechanical behaviors as the structure changes. These papers focused on the oxygen nonstoichiometry determined by means of high temperature gravimetry of A-site and B-sited doped $LaCrO_3$. There seems seldom to investigate the charge compensation mechanisms for aliovalent cations doping on B (Cr) site of $(La_{0.8}Ca_{0.2})CrO_{3-\delta}$ from the concept of defect chemistry. In this study, the charge compensation mechanisms and defect formation for Al, Co, Cu, and Fe-doping on the B site of $La_{0.8}Ca_{0.2}CrO_{3-\delta}$ were investigated systematically. The information of charge compensation mechanisms and defect formation may be valuable for a better understanding of the interconnect of $(La_{0.8}Ca_{0.2})CrO_{3-\delta}$-based ceramics used for SOFCs.

2. Experimental procedures

2.1. Sample synthesis

The $La_{0.8}Ca_{0.2}Cr_{0.9}M_{0.1}O_{3-\delta}$ (M = Al, Co, Cu, Fe) powders used for sintering characteristics were prepared by the solid-state technique. Stichiometric amounts of lanthanum oxide (La_2O_3, 99.9%), calcium carbonate ($CaCO_3$, 99.9%), chromium oxide (Cr_2O_3, 99.9%), aluminum oxide (Al_2O_3, 99.9%), cobalt oxide (Co_3O_4, 99.9%), copper oxide (CuO, 99.9%), and ferric oxide (Fe_2O_3, 99.9%) powders (as seen in Table 1) were mixed with distilled water for 12 h and then calcined in air at 1000 °C for 4 h. The powder samples were then pelletized. The pellets were dry pressed at 100 MPa using as-prepared powder for sintering. Sintering was carried out in air at 1500 °C for 6 h with a programmed heating rate of 5 °C/min. The sintered samples were over 90% of the theoretical density in all the specimens. Rectangular bar specimens (5 mm × 5 mm × 10 mm) were used for electrical conductivity measurements.

Table 1
Composition and abbreviation of $(La_{0.8}Ca_{0.2})Cr_{0.9}M_{0.1}O_{3-\delta}$ specimens.

Composition	Abbreviation
$(La_{0.8}Ca_{0.2})CrO_{3-\delta}$	LCCO
$(La_{0.8}Ca_{0.2})Cr_{0.9}Al_{0.1}O_{3-\delta}$	LCCO(Al)
$(La_{0.8}Ca_{0.2})Cr_{0.9}Co_{0.1}O_{3-\delta}$	LCCO(Co)
$(La_{0.8}Ca_{0.2})Cr_{0.9}Cu_{0.1}O_{3-\delta}$	LCCO(Cu)
$(La_{0.8}Ca_{0.2})Cr_{0.9}Fe_{0.1}O_{3-\delta}$	LCCO(Fe)

2.2. Characterization measurements

A computer interface X-ray powder diffractometer (XRD; Model Rigaku D/Max-II, Tokyo, Japan) with Cu K_α radiation ($\lambda = 0.15418$ nm) was used to identify the crystalline phase. The electrical conductivity measurements were made in the range of 300–850 °C by using the direct current (DC) four-probe technique in air and 5% H_2–95% Ar forming gas. The electrical conductivity measurements in air or 5% H_2–95% Ar, the soaking time before measurement is 1 h to reach heat balance. Four Ag leads were attached to the sample with Ag paste and fired at 800 °C.

3. Results and discussion

The tolerance factor is an index to evaluate the stability of forming the perovskite structure. The tolerance factor (t) of perovskite is expressed in the following equation:

$$t = \frac{r_A + r_O}{\sqrt{2}(r_B + r_O)}$$

where r_A, r_B, and r_O are the radii of A^{3+}, B^{3+}, and O^{2-} ions in ABO_3 perovskite, respectively. As the tolerance factor approaches one, the perovskite structure approaches ideal cubic symmetry. In this study, r_A is the radii of A site cations with coordination number of 8 ($La^{3+} = 1.18$, and $Ca^{2+} = 1.12$ Å), r_B is the radii of B site cations with coordination number of 6 ($Cr^{3+} = 0.62$, $Al^{3+} = 0.54$, $Co^{3+} = 0.55$, $Cu^{2+} = 0.73$, and $Fe^{3+} = 0.65$ Å), and the radius of oxygen ion O^{2-} with coordination number of 6 is 1.38 Å, respectively. The tolerance factors in the perovskite system are listed in Table 2. The values of tolerance factor vary from 0.8174 to 0.8247 with different cations in B (Cr) site of $(La_{0.8}Ca_{0.2})CrO_{3-\delta}$. The tolerance factors of are all greater than 0.81, indicating the perovskite is not distorted with different cations (Al^{3+}, Co^{3+}, Cu^{2+}, and Fe^{3+}) substitution for B site of $(La_{0.8}Ca_{0.2})CrO_{3-\delta}$. This behavior conforms to our XRD analysis as shown in Fig. 1 revealing the XRD patterns of the $(La_{0.8}Ca_{0.2})CrO_{3-\delta}$-based specimens sintered at 1500 °C. Generally, $LaCrO_3$-type perovskite has two phases with orthorhombic and rhombohedral

Table 2
Lattice parameters, Miller indices, corresponding 2-theta angle, cell volumes, crystal symmetries, and tolerance factor of $(La_{0.8}Ca_{0.2})CrO_{3-\delta}$-based specimens.

Composition	Miller indices	Corresponding 2-theta (°)	Lattice parameter (Å)	Cell volume (Å^3)	Crystal symmetries	Tolerance factor
LCCO	(1 1 2)	32.84	a = 5.457(3)	229.02	Orthorhombic	0.8218
	(0 0 4)	47.16	b = 5.449(2)			
	(0 2 4)	58.66	c = 7.702(3)			
LCCO(Al)	(1 1 2)	32.86	a = 5.424(2)	228.12	Orthorhombic	0.8232
	(0 0 4)	47.08	b = 5.452(4)			
	(0 2 4)	58.58	c = 7.714(3)			
LCCO(Co)	(1 1 2)	32.86	a = 5.424(4)	228.22	Orthorhombic	0.8247
	(0 0 4)	47.10	b = 5.456(3)			
	(0 2 4)	58.58	c = 7.712(2)			
LCCO(Cu)	(1 1 2)	32.66	a = 5.482(4)	232.74	Orthorhombic	0.8174
	(0 0 4)	46.90	b = 5.484(4)			
	(0 2 4)	58.30	c = 7.742(6)			
LCCO(Fe)	(1 1 2)	32.80	a = 5.458(2)	229.43	Orthorhombic	0.8206
	(0 0 4)	47.00	b = 5.440(3)			
	(0 2 4)	58.56	c = 7.727(1)			

symmetries. At room temperature $LaCrO_3$ has a distorted perovskite structure. The crystal structure transforms from orthorhombic to rhombohedral symmetry at 260 °C. In this study, no secondary phases were detected and all the specimens showed a single phase of orthorhombic perovskite crystal structure with a space group of *Pbnm*. In the unit cell of $(La_{0.8}Ca_{0.2})CrO_3$, the 4c sites in this structure are occupied by La and Ca. The 4b site is occupied by Cr and the O anions are located at 4c and 8d sites. The lattice parameters, unit cell volume, and crystal symmetries determined by Rietveld analysis from the corresponding XRD patterns are systematically presented in Table 2, in which the lattice parameters were calculated from the Miller indices of (1 1 2), (0 0 4), and (0 2 4). The introduction of different cations (Al^{3+}, Co^{3+}, Cu^{2+}, and Fe^{3+}) substitution for B-site of $La_{0.8}Ca_{0.2}CrO_{3-\delta}$ can cause a small shift in the $La_{0.8}Ca_{0.2}CrO_{3-\delta}$ peaks. This shift is indicative of change in lattice parameter. Since the radii of Al^{3+}, Co^{3+}, Cu^{2+}, and Fe^{3+} are much less than that of A site of La^{3+}, it is assumed that these cations entirely substitute for B site of Cr^{3+}. The cell volumes of LCCO(Al) and LCCO(Co) are both less than that of LCCO, it is suggested that the cation radii of Al^{3+} (0.54 Å) and Co^{3+} (0.55 Å) are smaller than Cr^{3+} (0.62 Å) in B site of $(La_{0.8}Ca_{0.2})CrO_{3-\delta}$. Contrarily, the cell volume of LCCO(Cu) and LCCO(Fe) are both larger than that of LCCO, it is ascribed to the fact that the cation radii of Cu^{2+} (0.73 Å) and Fe^{3+} (0.65 Å) are greater than Cr^{3+} (0.62 Å).

The Arrhenius plot for the electrical conductivity in air of $(La_{0.8}Ca_{0.2})CrO_{3-\delta}$-based specimens is plotted in Fig. 2. The linearity can be found between ln (σT) versus 1/T for all specimens. This indicates that the electrical conductivity in air obeys Arrhenius behavior. The electrical conductivity values in air and activation energy for all specimens are listed in Table 3. With temperature increase, the hopping of small polarons increase, and consequently the electrical conductivities increase at high temperature in all specimens, implying that the electrical conduction occurs by thermal activated by hopping of small polarons [15]. Comparison with all specimens, it is found that LCCO(Co) has the maximum conductivity value ($\sigma_{850\ ^\circ C} \sim 59.59$ S/cm) and the minimum activation energy (E_a = 11.42 kJ/mol). The electrical conductivities in air of

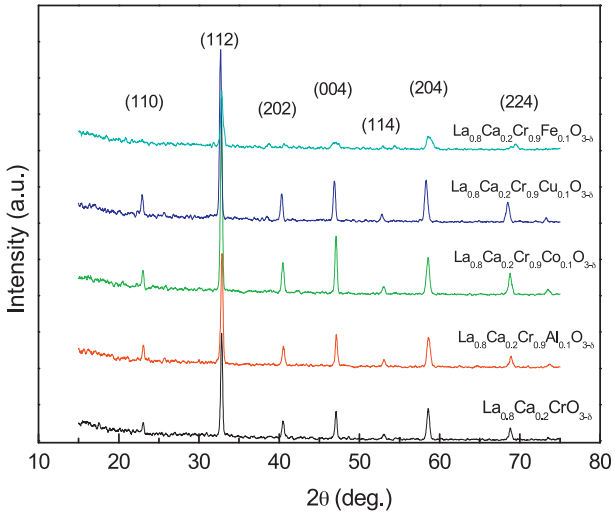

Fig. 1. X-ray diffraction patterns of $(La_{0.8}Ca_{0.2})CrO_{3-\delta}$-based specimens sintered at 1500 °C for 6 h.

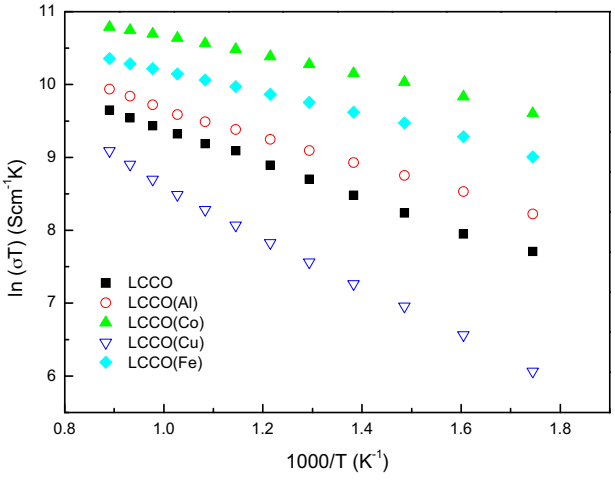

Fig. 2. The Arrhenius plot for the electrical conductivity in air of $(La_{0.8}Ca_{0.2})CrO_{3-\delta}$-based specimens.

Table 3
Electrical conductivity and activation energy of $(La_{0.8}Ca_{0.2})CrO_{3-\delta}$-based specimens in air.

Composition	Conductivity in air (S/cm)			Activation energy E_a (kJ/mol)
	750 °C	800 °C	850 °C	
LCCO	16.67	17.44	18.24	19.28
LCCO(Al)	22.28	23.48	24.33	16.16
LCCO(Co)	58.21	58.92	59.59	11.42
LCCO(Cu)	7.99	9.18	10.42	28.81
LCCO(Fe)	36.52	36.63	37.01	12.73

$(La_{0.8}Ca_{0.2})(Cr_{0.9}M_{0.1})O_{3-\delta}$ at temperature of 850 °C are ranked as follows, LCCO(Co) > LCCO(Fe) > LCCO(Al) > LCCO > LCCO(Cu). Activation energy for conduction is obtained by plotting the electrical conductivity data in Arrhenius relation for thermally activated conduction. Contrarily, the activation energy of $(La_{0.8}Ca_{0.2})(Cr_{0.9}M_{0.1})O_{3-\delta}$ in air in the temperature range of 300–850 °C are ranked as follows: LCCO(Cu) > LCCO > LCCO(Al) > LCCO(Fe) > LCCO(Co).

The temperature dependence of electrical conductivity of $(La_{0.8}Ca_{0.2})CrO_{3-\delta}$-based specimens in 5% H_2–95% Ar is shown in Fig. 3, which data as shown in Table 4. According to the conductivity behaviors, they can be grouped into two types. First type includes LCCO, LCCO(Al), LCCO(Cu),and LCCO(Co), the second type contains only LCCO(Fe). For the first type, the electrical conductivity increases with increasing temperature in the temperature range of 300–850 °C, indicating a small-polaron type conduction mechanism, in which the motion of carriers is thermally activated. For the second type, at low temperature, the electrical conduction mechanism obeys a small-polaron type, whereas at high temperature and low oxygen activity, lattice oxygen may significantly lost and the concentration of carrier is diminished resulting in the decrease in the electrical conductivity. In this case, the conduction mechanism transforms at the temperature of 600 °C for LCCO(Fe).

In this study, the concept of defect chemistry is used to explain the mechanism of electrical conductivity and discussed as

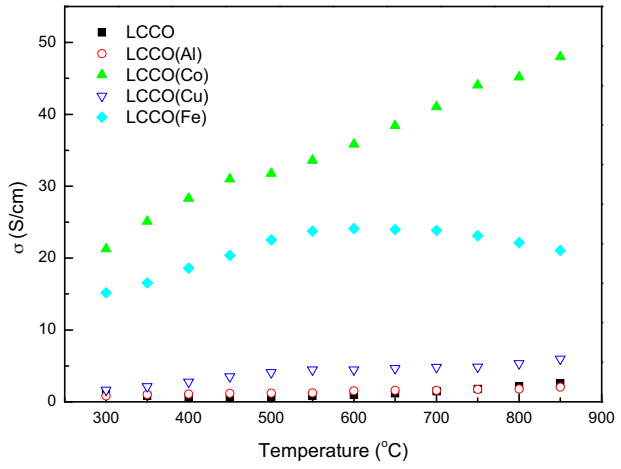

Fig. 3. Electrical conductivities of $(La_{0.8}Ca_{0.2})CrO_{3-\delta}$-based specimens as function of temperature in 5% H_2–95% Ar forming gas.

Table 4
Electrical conductivity of $(La_{0.8}Ca_{0.2})CrO_{3-\delta}$-based specimens in 5% H_2–95% Ar forming gas.

Composition	Conductivity in 5% H_2–95% Ar (S/cm)		
	750 °C	800 °C	850 °C
LCCO	1.80	2.17	2.60
LCCO(Al)	1.72	1.78	2.06
LCCO(Co)	44.04	45.18	47.98
LCCO(Cu)	4.27	5.36	5.98
LCCO(Fe)	23.12	22.14	21.05

follows. The electrical conductivity in $LaCrO_3$ is essentially due to the 3d band of the Cr ions [18]. Substitution with a lower-valence ion on the either A (La) or B (Cr) sites of $LaCrO_3$ may be the formation of Cr^{4+} and oxygen vacancies. However, electrical conductivity can be enhanced only the existence of Cr^{4+}. Oxygen vacancies have no additional contribution to the electrical conductivity. The formation of Cr^{4+} belongs to electronic compensation, whereas the formation of oxygen vacancies belongs to ionic compensation. Whether such a substitution favor either electronic or ionic compensation will depend on the conditions which equilibration of $LaCrO_3$ takes place [19]. For simplicity, it is assumed that p-type disorder predominates in nonstoichiometric $LaCrO_3$, and all defects are fully ionized. Using Kroger–Vink notation, the formation of Schottky defect is expressed by

$$null \Leftrightarrow V'''_{La} + V'''_{Cr} + 3V^{\bullet\bullet}_{O} \quad (1)$$

The p-type nonstoichiometric reaction is given by

$$\frac{3}{2}O_2 \Leftrightarrow V'''_{La} + V'''_{Cr} + 3O^{x}_{O} + 6h^{\bullet} \quad (2)$$

It is assumed that the acceptor dopant, Ca^{2+}, substituting for La^{3+}on a normal site. The ratio of cation stoichiometry (La:Cr = 1:1) must remain constant unless the formation of a secondary phase. This indicates that the concentration of lanthanum vacancies is equal to that of chromium vacancies. The electrical neutrality condition is given by

$$2[V^{\bullet\bullet}_{O}] + p = 3[V'''_{Cr}] + [Ca'_{La}] + 3[V'''_{La}] \quad (3)$$

At high oxygen activity, it is assumed that the concentration of intrinsic defects, *i.e.* $[V^{\bullet\bullet}_{O}]$, $[V'''_{Cr}]$ and $[V'''_{La}]$ are smaller compared with the solute, *i.e.* $[Ca'_{La}]$, the electroneutrality condition becomes

$$p = [Ca'_{La}] \quad (4)$$

At low oxygen activity, oxygen may be lost and ionic compensation may be take place through the formation of oxygen vacancies, the electroneutrality condition becomes

$$p = [Ca'_{La}] - 2[V^{\bullet\bullet}_{O}] \quad (5)$$

In general case, the defect chemical reaction can be expressed as:

$$La_{1-y}Ca'_{La_y}Cr_{1-y}Cr^{\bullet}_{Cr_y}O_3 \underset{\text{oxidation}}{\overset{\text{reduction}}{\rightleftharpoons}} L$$

$$a_{1-y}Ca'_{La_y}Cr_{1-y+2\delta}Cr^{\bullet}_{Cr_{y-2\delta}}O_{3-\delta} + \frac{\delta}{2}O_2 \quad (6)$$

where y is Ca-doping level and δ is the concentration of oxygen vacancies. In case of $y = 0.2$, the defect chemical reaction becomes

$$La_{0.8}Ca'_{La_{0.2}}Cr_{0.8}Cr^{\bullet}_{Cr_{0.2}}O_3 \underset{\text{oxidation}}{\overset{\text{reduction}}{\rightleftharpoons}} La_{0.8}Ca'_{La_{0.2}}Cr_{0.8+2\delta}Cr^{\bullet}_{Cr_{0.2-2\delta}}O_{3-\delta} + \frac{\delta}{2}O_2 \quad (7)$$

In this study, isovalent and aliovalent dopants substitute for B (Cr) site of $(La_{0.8}Ca_{0.2})CrO_{3-\delta}$ were used to investigate the conductivity mechanisms as discussed as follows.

(1) For isovalent dopant in B site of $(La_{0.8}Ca_{0.2})CrO_{3-\delta}$, it is assumed that trivalence cation substituting for Cr^{3+}on a normal site.

The electrical neutrality condition is similar to $(La_{0.8}Ca_{0.2})CrO_{3-\delta}$ as given by

$$2[V^{\bullet\bullet}_O] + p = 3[V'''_{Cr}] + [Ca'_{La}] + 3[V'''_{La}] \quad (8)$$

At high oxygen activity, it is assumed that the concentration of intrinsic defects, *i.e.* $[V^{\bullet\bullet}_O]$ and $[V'''_{La}]$ are smaller compared with the solute, *i.e.* $[Ca'_{La}]$, the electroneutrality condition becomes

$$p = [Ca'_{La}] \quad (9)$$

At low oxygen activity, oxygen may be lost and ionic compensation may be take place through the formation of oxygen vacancies, the electroneutrality condition becomes

$$p = [Ca'_{La}] - 2[V^{\bullet\bullet}_O] \quad (10)$$

In general case, the defect chemical reaction can be expressed as:

$$La_{1-y}Ca'_{La_y}Cr_{1-y-z}Cr^{\bullet}_{Cr_y}M^{x}_{Cr_z}O_3 \underset{\text{oxidation}}{\overset{\text{reduction}}{\rightleftharpoons}} La_{1-y}Ca'_{La_y}Cr_{1-y-z+2\delta}Cr^{\bullet}_{Cr_{y-2\delta}}M^{x}_{Cr_z}O_{3-\delta} + \frac{\delta}{2}O_2 \quad (11)$$

where y is Ca-doping level, z is trivalence cation-doping level, and δ is the concentration of oxygen vacancies. In case of $y = 0.2$, $z = 0.1$, and M = Al^{3+}, Co^{3+}, Fe^{3+}, the defect chemical reaction can be expressed as follows, respectively.

$$La_{0.8}Ca'_{La_{0.2}}Cr_{0.7}Cr^{\bullet}_{Cr_{0.2}}Al^{x}_{Cr_{0.1}}O_3 \underset{\text{oxidation}}{\overset{\text{reduction}}{\rightleftharpoons}} La_{0.8}Ca'_{La_{0.2}}Cr_{0.7+2\delta}Cr^{\bullet}_{Cr1}Al^{x}_{Cr_{0.1}}O_{3-\delta} + \frac{\delta_1}{2}O_2 \quad (12)$$

$$La_{0.8}Ca'_{La_{0.2}}Cr_{0.7}Cr^{\bullet}_{Cr_{0.2}}Co^{x}_{Cr_{0.1}}O_3 \underset{\text{oxidation}}{\overset{\text{reduction}}{\rightleftharpoons}} La_{0.8}Ca'_{La_{0.2}}Cr_{0.7+2\delta}Cr^{\bullet}_{Cr_{0.2-2\delta}}Co^{x}_{Cr_{0.1}}O_{3-\delta} + \frac{\delta_2}{2}O_2 \quad (13)$$

$$La_{0.8}Ca'_{La_{0.2}}Cr_{0.7}Cr^{\bullet}_{Cr_{0.2}}Fe^{x}_{Cr_{0.1}}O_3 \underset{\text{oxidation}}{\overset{\text{reduction}}{\rightleftharpoons}} La_{0.8}Ca'_{La_{0.2}}Cr_{0.7+2\delta}Cr^{\bullet}_{Cr_{0.2-2\delta}}Fe^{x}_{Cr_{0.1}}O_{3-\delta} + \frac{\delta_3}{2}O_2 \quad (14)$$

Although the defect chemical reaction of isovalent dopant in B site of $(La_{0.8}Ca_{0.2})CrO_{3-\delta}$ is similar to that Ca doped on A site of $LaCrO_{3-\delta}$ and the concentration of electron hole at high oxygen activity is the same as 0.2, at low oxygen activity is the same as 0.22δ, their conductivity behaviors are quit different.

The electrical conductivity σ for p-type conductor is given by

$$\sigma = e\mu p \quad (15)$$

where e is the electron charge, μ is the mobility of electron hole, and p is the concentration of electron hole. Because $(La_{0.8}Ca_{0.2})CrO_{3-\delta}$ perovskites belong to p-type conductor, the electrical conductivity is determined by Eq. (15). If it is assumed μ is a constant at fixed temperature, the electrical conductivity σ is determined by concentration of electron hole. In this case, the concentration of electron hole is equal to 0.2 at high oxygen activity, whereas, the concentration of electron hole is equal to $0.2 - 2\delta$ at low oxygen activity. There are two viewpoints to investigate the electrical conductivity mechanisms for isovalent dopant in B site of $(La_{0.8}Ca_{0.2})CrO_{3-\delta}$. The first viewpoint is to discuss electrical conductivities at high and low oxygen activity. The concentration of electron hole at high oxygen activity ($p = 0.2$) is larger than that at low oxygen activity ($p = 0.2 - 2\delta$). Obviously, the electrical conductivities for isovalent dopant in B site of $(La_{0.8}Ca_{0.2})CrO_{3-\delta}$ in air are larger than those in 5% H_2–95% Ar. The second viewpoint is to discuss the relationship between the electrical conductivities and the kind of dopant. From the defect chemical reactions, Eqs. (7) and (12)–(14), it is assumed that the compensation mechanism completely dominated by electrical compensation and the concentration of electron hole should to be $0.2 + u$ at high oxygen activity. But in reality the electrical conductivities in air significantly varied with the kind of dopant. We suspected that (1) the compensation mechanisms contain ionic and electrical compensation at high oxygen activity and (2) as the percentage of ionic compensation is increased, the electrical conductivity is decreased. For ionic compensation, it is assumed that trivalent cations (Al^{3+}, Co^{3+}, Fe^{3+}) were doped on B (Cr) site of $(La_{0.8}Ca_{0.2})CrO_{3-\delta}$, the defect chemical reaction can be expressed as:

$$Al_2O_3 \overset{(La_{0.8}Ca_{0.2})CrO_3}{\longrightarrow} 2Al^{x}_{Cr} + 2V'''_{Cr} + 3V^{\bullet\bullet}_O + 3O^{X}_O \quad (16)$$

$$Co_2O_3 \overset{(La_{0.8}Ca_{0.2})CrO_3}{\longrightarrow} 2Co^{x}_{Cr} + 2V'''_{Cr} + 3V^{\bullet\bullet}_O + 3O^{X}_O \quad (17)$$

$$Fe_2O_3 \overset{(La_{0.8}Ca_{0.2})CrO_3}{\longrightarrow} 2Fe^{x}_{Cr} + 2V'''_{Cr} + 3V^{\bullet\bullet}_O + 3O^{X}_O \quad (18)$$

The prevailing compensation mechanism (electrical or ionic) will depend on the kind of dopant, oxygen activity, and temperature. Clearly, at high oxygen activity and higher temperature, the compensation mechanism is significantly dominated by the formation of oxygen vacancy, *i.e.* ionic compensation. It is suggested that the compensation mechanisms contained ionic and electrical compensations,

and the compensation ratios of *electrical/ionic* are quite different for $(La_{0.8}Ca_{0.2})CrO_{3-\delta}$-based specimens. Based on the result of electrical conductivity in air, the compensation ratio of *electrical/ionic* can be ranked as follows:

$$LCCO(Co) > LCCO(Fe) > LCCO(Al) > LCCO$$

At low oxygen activity, the electrical conductivities of $(La_{0.8}Ca_{0.2})CrO_{3-\delta}$-based specimens are determined by the concentration of electron hole. In case of isovalent dopant in B site of $(La_{0.8}Ca_{0.2})CrO_{3-\delta}$, the concentrations of electron hole are all the same as $0.2 - 2\delta$. On the basis of the result of electrical conductivities in 5% H_2–95% Ar and the defect chemical reactions, Eqs. (7) and (12)–(14), it is suggested that the formation of the concentration of oxygen vacancies are quite different for $(La_{0.8}Ca_{0.2})CrO_{3-\delta}$-based specimens. It is presumed that the concentration of oxygen vacancies of LCCO(Co) is lowest with large electrical conductivity, the concentration of oxygen vacancies of LCCO(Al) is highest with small electrical conductivity. For isovalent dopant in B site of $(La_{0.8}Ca_{0.2})CrO_{3-\delta}$, in 5% H_2–95% Ar, the formation of oxygen vacancies can be ranked as follows:

$$LCCO(Al) > LCCO > LCCO(Fe) > LCCO(Co)$$

(2) For acceptor dopant in B site of $(La_{0.8}Ca_{0.2})CrO_{3-\delta}$, it is assumed that divalence cation substituting for Cr^{3+}on a normal site. In case of $(La_{0.8}Ca_{0.2})Cr_{0.9}Cu_{0.1}O_{3-\delta}$, the electrical neutrality condition can be expressed as:

$$2[V_O^{\bullet\bullet}] + p = 3[V_{Cr}'''] + [Ca_{La}'] + 3[V_{La}'''] + [Cu_{Cr}'] \quad (19)$$

At high oxygen activity, it is assumed that the concentration of intrinsic defects, *i.e.* $[V_O^{\bullet\bullet}]$, $[V_{Cr}''']$ and $[V_{La}''']$ are smaller compared with the solute, *i.e.* $[Ca_{La}']$ and $[Cu_{Cr}']$, the electroneutrality condition becomes

$$p = [Ca_{La}'] + [Cu_{Cr}'] \quad (20a)$$

At low oxygen activity, oxygen may be lost and ionic compensation may be take place through the formation of oxygen vacancies, the electroneutrality condition becomes

$$p = [Ca_{La}'] + [Cu_{Cr}'] - 2[V_O^{\bullet\bullet}] \quad (20b)$$

In general case, the defect chemical reaction can be expressed as:

$$La_{1-y}Ca_{La_y}'Cr_{1-y-2z}Cr_{Cr_{y+z}}^{\bullet}M_{Cr_z}'O_3 \underset{\text{oxidation}}{\overset{\text{reduction}}{\longrightarrow}} La_{1-y}Ca_{La_y}'Cr_{1-y-2z+2\delta}Cr_{Cr}^{\bullet}Cr_{Cr_{y+z-2\delta}}M_{Cr_z}'O_{3-\delta} + \frac{\delta}{2}O_2 \quad (21)$$

where y is Ca-doping level, z is divalence cation-doping level, and δ is the concentration of oxygen vacancies. In case of $y = 0.2$, $z = 0.1$, and $M = Co^{2+}$, Cu^{2+}, Fe^{2+}, the defect chemical reaction can be expressed as follows, respectively.

$$La_{0.8}Ca_{La_{0.2}}'Cr_{0.6}Cr_{Cr_{0.3}}^{\bullet}Co_{Cr_{0.1}}'O_3 \underset{\text{oxidation}}{\overset{\text{reduction}}{\longrightarrow}} La_{0.8}Ca_{La_{0.2}}'Cr_{0.6+2\delta}Cr_{Cr_{0.3-2\delta}}^{\bullet}Co_{Cr_{0.1}}'O_{3-\delta} + \frac{\delta_4}{2}O_2 \quad (22)$$

$$La_{0.8}Ca_{La_{0.2}}'Cr_{0.6}Cr_{Cr_{0.3}}^{\bullet}Cu_{Cr_{0.1}}'O_3 \underset{\text{oxidation}}{\overset{\text{reduction}}{\longrightarrow}} La_{0.8}Ca_{La_{0.2}}'Cr_{0.6+2\delta}Cr_{Cr_{0.3-2\delta}}^{\bullet}Cu_{Cr_{0.1}}'O_{3-\delta} + \frac{\delta_5}{2}O_2 \quad (23)$$

$$La_{0.8}Ca_{La_{0.2}}'Cr_{0.6}Cr_{Cr_{0.3}}^{\bullet}Fe_{Cr_{0.1}}'O_3 \underset{\text{oxidation}}{\overset{\text{reduction}}{\longrightarrow}} La_{0.8}Ca_{La_{0.2}}'Cr_{0.6+2\delta}Cr_{Cr_{0.3-2\delta}}^{\bullet}Fe_{Cr_{0.1}}'O_{3-\delta} + \frac{\delta_6}{2}O_2 \quad (24)$$

In these cases, at high oxygen activity, the concentrations of electron hole all are equal to 0.3, at low oxygen activity, the concentrations of electron hole all are equal to $0.3 - 2\delta$. However, their electrical conductivity values are quite different. At high oxygen activity, the defect chemical reactions, Eqs. (22)–(24) show the compensation mechanism completely dominated by electrical compensation. But in reality the electrical conductivities in air significantly varied with the kind of dopant. We suspected that (1) the compensation mechanisms contain ionic and electrical compensation and (2) the ratios of electrical to ionic compensation are quite different. For ionic compensation, it is assumed that divalent cations (Co^{2+}, Cu^{2+}, Fe^{2+}) were doped on B (Cr) site of $(La_{0.8}Ca_{0.2})CrO_{3-\delta}$, the defect chemical reactions can be expressed as:

$$2CoO \overset{(La_{0.8}Ca_{0.2})CrO_3}{\longrightarrow} 2Co_{Cr}' + V_O^{\bullet\bullet} + 2O_O^X \quad (25)$$

$$2CuO \overset{(La_{0.8}Ca_{0.2})CrO_3}{\longrightarrow} 2Cu_{Cr}' + V_O^{\bullet\bullet} + 2O_O^X \quad (26)$$

$$2FeO \overset{(La_{0.8}Ca_{0.2})CrO_3}{\longrightarrow} 2Fe_{Cr}' + V_O^{\bullet\bullet} + 2O_O^X \quad (27)$$

Clearly, at high oxygen activity and higher temperature, the compensation mechanism is significantly dominated by the formation of oxygen vacancy, *i.e.* ionic compensation. It is suggested that the compensation ratios of *electrical/ionic* are quite different for $(La_{0.8}Ca_{0.2})CrO_{3-\delta}$-based specimens. Based on the result of electrical conductivity in air, the compensation ratio of *electrical/ionic* can be ranked as follows:

$$LCCO(Co) > LCCO(Fe) > LCCO(Cu) > LCCO$$

At low oxygen activity, the electrical conductivities of $(La_{0.8}Ca_{0.2})CrO_{3-\delta}$-based specimens are determined by the concentration of electron hole. In 5% H_2–95% Ar, On the basis of the result of electrical conductivities in 5% H_2–95% Ar and the defect chemical reactions Eqs. (22)–(24), it is suggested that the formation of the concentration of oxygen vacancies varied with the kind of dopant. In case of acceptor dopant in B site of $(La_{0.8}Ca_{0.2})CrO_{3-\delta}$, the concentrations

of electron hole are all the same as $0.3 - 2\delta$. It is presumed that the concentration of oxygen vacancies of LCCO(Co) is lowest with large electrical conductivity, the concentration of oxygen vacancies of LCCO is highest with small electrical conductivity. The formation concentration of oxygen vacancies can be ranked as follows:

$$\text{LCCO} > \text{LCCO(Cu)} > \text{LCCO(Fe)} > \text{LCCO(Co)}$$

Because the transition metals with multiple valences (divalence and trivalence) such as Co and Fe, they may act as isovalent and acceptor dopants in substitution for Cr in $(La_{0.8}Ca_{0.2})CrO_{3-\delta}$ specimens. The ratios of divalence/trivalence are difficult to determine for Co and Fe in LCCO(Co) and LCCO(Fe), respectively. However, the extents of divalence for Co and Fe are significant effect on their conductivities at low oxygen activity. If it is assumed that (1) the electrical conductivities are determined by the concentration of electron hole, (2) before reduction and acceptor doping in B site, Cr entirely exists in the form of Cr^{3+} for $(La_{0.8}Ca_{0.2})CrO_{3-\delta}$-based specimens. It is speculated that the extent of Co^{2+} in LCCO(Co) is large than that in the form of Co^{3+}. This is due to the fact that at low oxygen activity, the concentrations of electron hole all are equal to $0.3 - 2\delta$ for acceptor doping, whereas he concentrations of electron hole all are equal to $0.2 - 2\delta$ for isovalent doping. According the result of electrical conductivity in 5% H_2–95% Ar, the ratio of Co^{2+}/Co^{3+} is larger than that of Fe^{2+}/Fe^{3+}. In Fig. 3, it is worth to notice that the transformation temperature occur at LCCO(Fe). This transformation temperature indicates that change in prevailing compensation mechanism. There are two possible mechanisms. The first possibility is the change of prevailing compensation mechanism. In this case, above the transformation temperature, the prevailing compensation mechanism changes from the electrical to ionic compensation. The second possibility is the variation in the ratio of Co^{2+}/Co^{3+}. In this case, the ratio of Co^{2+}/Co^{3+} significantly decreases when the temperature above the transformation temperature.

4. Conclusions

In this study, the electrical conduction behaviors of $(La_{0.8}Ca_{0.2})CrO_{3-\delta}$-based specimens in high and low oxygen activities were investigated systematically. The conductivities of $(La_{0.8}Ca_{0.2})CrO_{3-\delta}$-based specimens are decreased in reducing atmosphere than those in air. This is due to the fact that oxygen may be lost and ionic compensation may be take place through the formation of oxygen vacancies and the electrical compensation may arise by changing the valence of Cr in which Cr will take from tri-valence to tetra-valence in reducing atmosphere. However the formation of oxygen vacancies has no contribution to electrical conductivity, the compensation mechanism is dominated by the electrical compensation, *i.e.* the take place a transition of $Cr^{3+} \rightarrow Cr^{4+}$ rather than that of ionic compensation, *i.e.* the formation of oxygen vacancies. Based on the defect chemical reactions and the results of electrical conductivity, the concentration of electron hole at high oxygen activity is larger than that at low oxygen activity. Therefore the electrical conductivity of $(La_{0.8}Ca_{0.2})CrO_{3-\delta}$-based ceramics at air is larger than that at 5% H_2–95% Ar forming gas. The compensation mechanisms contain ionic and electrical compensation and the ratios of electrical to ionic compensation varied with the kind of dopant which significantly effects the electrical conductivity.

Acknowledgements

The authors thank the National Science Council of Taiwan for financially supporting this research under Contract No. NSC 98-2213-M-259-002.

References

[1] D. Sanchez, R. Chacartegui, A. Munoz, T. Sanchez, On the effect of methane internal reforming modeling in solid oxide fuel cells, Int. J. Hydrogen Energy 33 (2008) 1834–1844.
[2] A. Pramuanjaroenkij, S. Kakac, X.Y. Zhou, Mathematical analysis of planar solid oxide fuel cells, Int. J. Hydrogen Energy 33 (2008) 2547–2565.
[3] Z. Yang, K.S. Weil, D.M. Paxton, J.W. Stevenson, Selection and evaluation of heat-resistant alloys for SOFC interconnects applications, J. Electrochem. Soc. 150 (2003) A1188–1201.
[4] W.Z. Zhu, S.C. Deevi, Development of interconnect materials for solid oxide fuel cells, Mater. Sci. Eng. A 348 (2003) 227–243.
[5] N.Q. Minh, T. Takahashi, Science and Technology of Ceramic Fuel Cells, Elsevier, Amsterdam, 1995, p. 165.
[6] S.C. Singhal, K. Kendall, High Temperature Solid Oxide Fuel Cells Fundamentals, Design and Applications, Elsevier, Amsterdam, 2003, p. 173.
[7] R.N. Basu, F. Tietz, O. Teller, E. Wessel, H.P. Buchkremer, D. Stocer, $LaNi_{0.6}Fe_{0.4}O_3$ as a cathode contact material for solid oxide fuel cells, J. Solid State Electrochem. 7 (2003) 416–420.
[8] A. Chakraborty, R.N. Basu, H.S. Maiti, Low temperature sintering of La(Ca)CrO_3 prepared by an autoignition process, J. Mater. Lett. 45 (2000) 162–166.
[9] L.P. Rivas-Vazquez, J.C. Rendon-Angeles, J.L. Rodriguez-Galicia, C.A. Gutierrez-Chavarria, K.J. Zhu, K. Yanagisawa, Preparation of calcium doped $LaCrO_3$ fine powders by hydrothermal method and its sintering, J. Eur. Ceram. Soc. 26 (2006) 81–88.
[10] S. Ghosh, A.D. Sharma, R.N. Basu, H.S. Maiti, Influence of B site substitutions on lanthanum calcium chromite nanocrystalline materials for a solid-oxide fuel cell, J. Am. Ceram. Soc. 90 (2007) 3741–3747.
[11] M. Mori, N.M. Sammes, Sintering and thermal expansion characterization of Al-doped and Co-doped lanthanum strontium chromites synthesized by Pechini method, Solid State Ionics 146 (2002) 301–312.
[12] M. Mori, Y. Hiei, T. Yamamoto, Control of thermal expansion of strontium doped lanthanum chromite perovskites by B-site doping for high temperature solid oxide fuel cell separators, J. Am. Ceram. Soc. 84 (2001) 781–786.
[13] W.J. Weber, C.W. Griffin, L. Bates, Effects of cation substitution on electrical and thermal transport properties of $YCrO_3$ and $LaCrO_3$, J. Am. Ceram. Soc. 70 (1987) 265–270.
[14] X. Ding, Y. Liu, L. Gao, L. Guo, Effect of cation substitution on thermal expansion and electrical properties of lanthanum chromites, J. Alloys Compd. 425 (2006) 318–322.
[15] M. Oishi, K. Yashiro, K. Sato, J. Mizusaki, T. Kawada, Oxygen non-stoichiometry and defect structure analysis of B-site mixed perovskite-type oxide (La, Sr)(Cr, M)$O_{3-\delta}$ (M = Ti, Mn and Fe), J. Solid State Chem. 181 (2008) 3177–3184.

[16] M. Oishi, K. Yashiro, J.O. Hong, Y. Nigara, T. Kawada, J. Mizusaki, Oxygen nonstoichiometry of B-site doped $LaCrO_3$, Solid State Ionics 178 (2007) 307–312.

[17] K. Hilpert, R.W. Steinbrech, F. Boroomand, E. Wessel, F. Meschke, A. Zuev, O. Teller, H. Nickel, L. Singheiser, Defect formation and mechanical stability of perovskites based on $LaCrO_3$ for solid oxide fuel cells (SOFC), J. Eur. Ceram. Soc. 23 (2003) 3009–3020.

[18] I.G. Austin, N.F. Mott, Polarons in crystalline and non-crystalline materials, Adv. Phys. 18 (1969) 41–102.

[19] B.K. Flandermeyer, M.M. Nasrallah, A.K. Agarwal, H.U. Anderson, Defect structure of Mg-doped $LaCrO_3$ model and thermogravimetric measurements, J. Am. Ceram. Soc. 67 (1984) 195–198.